Spatio-temporal characterization of few-cycle pulses obtained by filamentation

A. Zaïr[1*], A. Guandalini[1], F. Schapper[1], M. Holler[1], J. Biegert[i], L. Gallmann[1], U. Keller[1], A. Couairon[2], M. Franco[3], and A. Mysyrowicz[3]

[1]*ETH Zurich, Physics Department / Institute of Quantum Electronics, 8093 Zurich, Switzerland*
[2]*Centre de Physique Théorique, CNRS, École Polytechnique, F-91128 Palaiseau, France*
[3]*Laboratoire d'Optique Appliquée, École Nationale Supérieure des Techniques Avancées—École Polytechnique, F-91761 Palaiseau Cedex, France*
[*]Corresponding author: zair@phys.ethz.ch

Abstract. Intense sub-5-fs pulses were generated by filamentation in a noble gas and subsequent chirped-mirror pulse compression. The transversal spatial dependence of the temporal pulse profile was investigated by spatial selection of parts of the output beam. Selecting the central core of the beam is required for obtaining the shortest possible pulses. Higher energy efficiency is only obtained at the expense of pulse contrast since towards the outer parts of the beam the energy is spread into satellite structures leading to a double-pulse profile on the very off-axis part of the beam. Depending on the requirements for a particular application, a trade-off between the pulse duration and the pulse energy has to be done. The energy of the sub-5-fs pulses produced was sufficient for the generation of high order harmonics in Argon. In addition, full simulation is performed in space and time on pulse propagation through filamentation that explains the double-pulse structure observed as part of a conical emission enhanced by the plasma defocusing.

OCIS codes: (320.5520) Pulse Compression; (320.7100) Ultrafast Measurement

References and links

1. J. J. Macklin, J. D. Kmetec, and C. L. Gordon, "High-order harmonic generation using intense femtosecond pulses," Phys. Rev. Lett. **70,** 766-769 (1993).
2. Ph. Antoine, A. L'Huillier, and M. Lewenstein, "Attosecond Pulse Trains using High-Order Harmonics," Phys. Rev. Lett. **77,** 1234-1237 (1996).
3. M. Drescher, M. Hentschel, R. Kienberger, G. Tempea, C. Spielmann, G. A. Reider, P. B. Corkum, and F. Krausz, "X-ray pulses approaching the Attosecond Frontier," Science **291,** 1923-1927 (2001).
4. P. M. Paul, E. S. Toma, P. Breger, G. Mullot, F. Auge, Ph. Balcou, H. G. Muller, and P. Agostini, "Observation of Train of Attosecond Pulses from High Harmonic Generation," Science **292,** 1689-1692 (2001).
5. H. R. Telle, G. Steinmeyer, A. E. Dunlop, J. Stenger, D. H. Sutter, and U. Keller, "Carrier-envelope offset phase control: A novel concept for absolute optical frequency measurement and ultrashort pulse generation," Appl. Phys. B. **69,** 327-332 (1999).
6. D. J. Jones, S. A. Diddams, J. K. Ranka, A. Stentz, R. S. Windeler, J. L. Hall, and S. T. Cundiff, "Carrier-envelope phase control of Femtosecond Mode-locked lasers and direct optical frequency synthesis," Science **288,** 635-639 (2000).
7. G. Sansone, E. B., F. Calegari, C. Vozzi, L. Avaldi, R. Flammini, L. Poletto, P. Villoresi, C. Altucci, R. Velotta, S. Stagira, S. De Silvestri, and M. Nisoli, "Isolated single-cycle attosecond pulses," Science **314,** 443-446 (2006).
8. M. Nisoli, S. de Silvestri, O. Svelto, R. Szipöecs, K. Ferencz, Ch. Spielmann, S. Sartania, and F. Krausz "Compression of high-energy laser pulses below 5 fs," Opt. Lett. **22,** 522-524 (1997).
9. C. P. Hauri, W. Kornelis, F. W. Helbing, A. Heinrich, A. Couairon, A. Mysyrowicz, J. Biegert, U. Keller "Generation of intense carrier-envelope phase-locked few-cycle laser pulses through filamentation," Appl. Phys. B. **79,** 673-677 (2004).

#80983 - $15.00 USD Received 13 Mar 2007; revised 9 Apr 2007; accepted 10 Apr 2007; published 18 Apr 2007

10. A. Guandalini, P. Eckle, M. P. Anscombe, P. Schlup, J. Biegert, and U. Keller, "5.1 fs pulses generated by filamentation and carrier-envelope phase stability analysis," J. Phys. B: At. Mol. Opt. Phys. **39,** S257-S264 (2006).
11. A. Couairon, J. Biegert, C. P. Hauri, W. Kornelis, F. W. Helbing, U. Keller, and A. Mysyrowicz, "Self-compression of ultrashort laser pulses down to one optical cycle by filamentation," J. Mod. Opt. **53,** 87-96 (2006).
12. A. Apolonski, A. Poppe, G. Tempea, Ch. Spielmann, Th. Udem, R. Holzwarth, T. W. Hänsch and F. Krausz, "Controlling the phase evolution of few-cycle light pulses," Phys. Rev. Lett. **85,** 740-743 (2000).
13. A. Braun, G. Korn, X. Liu, D. Du, J. Squier, and G. Mourou, "Self-channeling of high-peak-power femtosecond laser pulses in air," Opt. Lett. **20,** (1995).
14. B. Prade, M. Franco, A. Mysyrowicz, A. Couairon, H. Buersing, B. Eberle, M. Krenz, D. Seiffer, and O. Vasseur, "Spatial mode cleaning by femtosecond filamentation in air," Opt. Lett. **31**, 2601-2603 (2006).
15. H. R. Lange, A. Chiron, J-F. Ripoche, A. Mysyrowicz, P. Breger, and P. Agostini, "High-Order Harmonic generation and quasiphase matching in Xenon using self-guided femtosecond pulses," Phys. Rev. Lett. **81,** 1611-1613 (1998).
16. A. Couairon, M. Franco, A. Mysyrowicz, J. Biegert, and U. Keller, "Pulse self-compression to the single-cycle limit by filamentation in a gas with a pressure gradient," Opt. Lett. **30,** 2657-2659 (2005).
17. G. Stibenz, N. Zhavoronkov, and G. Steinmeyer, "Self-compression of millijoule pulses to 7.8 fs duration," Opt. Lett. **3,** 274-276 (2006).
18. F. Théberge, N. Akŏzbek, W. Liu, A. Becker, and S. L. Chin, "Tunable ultrashort laser pulses generated through Filamentation in Gases," Phys. Rev. Lett. 023904 (2006).
19. L. Gallmann, T. Pfeifer, P. M. Nagel, M. J. Abel, D. M. Neumark, and S .R. Leone, "Comparaison of the filamentation and the hollw-core fiber characteristics for pulse compression into the few-cycle regime," App. Phys. B. **86,** 2503-2508 (2007).
20. L. Gallmann, D. H. Sutter, N. Matuschek, G. Steinmeyer, U. Keller, C. Iaconis, and I. A. Walmsley, "Characterization of sub-6-fs optical pulses with spectral phase interferometry for direct electric-field reconstruction," Opt. Lett. **24,** 1314-1316 (1999).
21. W. Kornelis, J. Biegert, J. W. G. Tisch, M. Nisoli, G. Sansone, C. Vozzi, S. De Silvestri, and U. Keller, "Single-shot kilohertz characterization of ultrashort pulses by spectral phase interferometry for direct electric-filed reconstruction," Opt. Lett. **28,** 281-283 (2003).
22. C. Iaconis and I. A. Walmsley, "Spectral phase interferometry for direct electric-field reconstruction of ultrashort optical pulses," Opt. Lett. **23,** 792-794 (1998).
23. P. Salières, B. Carré, L. Le Déroff, F. Grasbon, G. G. Paulus, H. Walther, R. Kopold, W. Becker, D. B. Miloevi, A. Sanpera, and M. Lewenstein, "Feynman's path-integral approach for intense-laser-atom interactions," Science **292,** 902 (2001).
24. A. L'Huillier, M. Lewenstein, P. Salières, Ph. Balcou, M. Yu. Ivanov, J. Larsson, and C. G. Wahlström, "High-order harmonic generation cutoff," Phys. Rev. A. **48,** R3433-R3436 (1993).
25. A. Couairon and A. Mysyrowicz, "Femtosecond filamentation in transparent media," Phys. Rep. **441,** 47-189 http://dx.doi.org/10.1016/j.physrep.2006.12.005 (2007).
26. T. Brabec and F. Krausz, "Nonlinear optical pulse Propagation in the Single-Cycle Regime," Phys. Rev. Lett. **78,** 3282 (1997).
27. A. A. Zozulya, S. A. Diddams, and T. S. Clement, "Investigatins of nonlinear femtosecond pulse propagation with the inclusion of Raman, shock, and third-order phase effects," Phys. Rev. A. **58,** 3303 (1998).
28. Dalgarno and Kingston, "The Refractive Indices and Verdet Constants of the Inert Gases," Proc. Roy. Soc. London Ser. A. **259,** (1966).
29. D. P. Shelton "Nonlinear-optical susceptibilities of gases measured at 1064 and 1319 nm," Phys. Rev. A. **42,** 2578 (1990).
30. V. Mizrahi and D. P. Shelton "Dispersion of Nonlinear Susceptibilities of Ar, N_2, and O_2 Measured and Compared," Phys. Rev. Lett. **55,** 696 (1985).
31. A. Couairon, M. Franco, G. Méchain, T. Olivier, B. Prade, and A. Mysyrowicz, "Fentosecond filamentation in air at low pressures," Opt. Commun. **265,** (2006).
32. K. Ishikawa, H. Kumagai, and K. Midorikawa, "High-power regime of femtosecond-laser pulse propagation in silica: Multiple-cone formation," Phys. Rev. E. **66,** 056608 (2002).
33. A. Dubietis, E. Gaižauskas, G. Tamŏsauskas, and P. Di Trapani, "Light Filaments without self-channeling," Phys. Rev. Lett. **92,** 253903 (2004).
34. D. Faccio, P. Di Trapani, S. Minardi, A. Bramati, F. Bragheri, C. Liberale, V. Degiorgio, A. Dubietis, and A. Matijosius, "Far-field spectral characterization of conical emission ans filamentation in Kerr media," J. Opt. Soc. Am. B. **22,** 862 (2005).
35. D. Faccio, A. Matijosius, A. Dubietis, R. Piskarskas, A. Varanavičius, E. Gaižauskas, A. Piskarskas, A. Couairon, and P. Di Trapani, "Near- and Far-field evolution of laser pulse filaments in Kerr media," Phys. Rev. E. **72,** 037601 (2005).
36. A. Couairon, E. Gaižauskas, D. Faccio, A. Dubietis, and P. Di Trapani, "Nonlinear X-wave formation by femtosecond filamentation in Kerr media," Phys. Rev. E. **73,** 016608 (2006).

#80983 - $15.00 USD Received 13 Mar 2007; revised 9 Apr 2007; accepted 10 Apr 2007; published 18 Apr 2007

1. Introduction

During the last decade, techniques for the generation of intense few-cycle laser pulses have emerged that led to dramatic improvements in many fields of research, and that have revolutionized high field physics and extreme nonlinear optics. High order harmonic generation (HHG) [1,2] is one of the applications for such short pulses, which has culminated in the generation of single attosecond pulses in the extreme ultraviolet region (XUV) [3]. HHG is the coherent up-conversion of optical frequencies into the XUV spectral region, and is typically achieved by strongly focusing an intense near-infrared driving pulse into a noble gas. Many-cycle driving pulses (> 30 fs) yielded attosecond pulse trains [4], whereas few-cycle pulses, paired with carrier envelope offset (CEO) phase stability [5,6], led to the generation of isolated attosecond pulses [3,7].

In the past, intense few-cycle pulses were nearly exclusively generated using gas-filled hollow fibers [8]. Recently, an alternative technique based on filamentation in a noble gas was demonstrated, which is simpler to implement and does not suffer from the draw-backs of coupling an intense pulse into a narrow and elongated waveguide [9]. The experimental arrangement and laser requirements for filamentation are similar to the previous technique, just with the hollow fiber being removed. As a result, implementation is extremely simple. The filament compression in the few-cycle regime is surprising because the high plasma density generated has such strong dispersion that a few-cycle laser pulse would be expected to broaden very fast. In addition, the CEO phase of the compressed pulse is maintained or even further stabilized, a fact one would not have expected. Meanwhile, simulations reproduce the experimental results well [9-12].

Filamentation is understood as a competition between several physical effects: Localization in the transverse diffraction plane results from the dynamics of the Kerr effect, that leads to beam focusing, and multi-photon absorption that leads to ionization and plasma induced beam defocusing [13]. Under appropriate laser parameters and ambient medium conditions, this competition can induce a self-guiding effect over several Rayleigh lengths, i.e. the beam takes the form of an intense narrow core during the nonlinear interaction with the medium, surrounded by a weak part propagating linearly. Similar to the hollow-fiber technique, self-phase modulation during filamentation broadens the incident pulse spectrum to more than an optical octave, while self-guiding acts as a spatial filter leading to an improvement in spatial mode quality [14]. Furthermore, since the pulse intensity is clamped inside the filament within a very narrow range [15], the intensity stability is improved by the process. The energy throughput tends to be slightly higher compared to the hollow fiber technique. The complex processes taking place during filamentation can lead to a variety of different effects, which more and more groups have begun to investigate recently. Of particular interest is the effect of self-compression to the few-cycle regime within the filament, which was predicted by numerical modeling [9, 11]. Theoretical analysis as well as numerical simulations suggest that the use of a longitudinally non-uniform gas distribution could lead to efficient self-compression down to the single-cycle limit, thereby eliminating the need for any external chirped mirror compression [16]. Power scaling to above 1 mJ has been demonstrated as well [17]. Another attractive aspect of filaments is the possibility to generate tunable ultrashort pulses by filamentation employing two-color driving fields and four-wave mixing [18].

As with most sources of few-cycle pulses, a certain spatial inhomogeneity is observed in the output from the filamentation, which is consistent with theoretical prediction [11]. In an earlier study, the lateral variation of the spectral content was investigated and compared to that of the hollow-core fiber technique [19]. Here, we demonstrate that the shortest pulses are only obtained with a careful selection of the central core of the emerging beam. In addition, we have performed spatially resolved measurements of the complete temporal structure of the filament beam using spectral phase interferometry for direct electric-field reconstruction

#80983 - $15.00 USD Received 13 Mar 2007; revised 9 Apr 2007; accepted 10 Apr 2007; published 18 Apr 2007

(SPIDER) [20-22]. The main result is that only the central core of the beam contains the few-cycle pulse with the surrounding beam structures still containing a significant amount of energy.
This investigation has been performed on sub-5-fs pulses which are, to our knowledge, currently the shortest pulses obtained through filamentation. These pulses are compressed from approximately 30 fs down to 10 fs in a first filamentation stage followed by chirped mirrors. The output of this first stage is then further shortened to below 5 fs by filamentation in a second cell and post-compression, which is needed to compensate for the dispersion.

2. Experiment

The parameter dependence of filamentation on the ambient medium and ingoing pulse characteristics has been reported previously [9]. Under optimized conditions, the result of filamentation is a beam with exceptional spatial quality ($M^2 \approx 1$), good pointing stability and a very broad spectrum covering up to more than one octave. We used our two-stage filamentation setup previously described in [9, 10]. A Ti:sapphire amplifier system provided 30-fs pulses centered at 795 nm with energies of up to 1 mJ at a repetition rate of 1 kHz. The input beam diameter was 6.2 mm (FWHM) and the input pulse from the amplifier was measured with SPIDER. Figure 1(a) shows the pulse shape in time and its associated spectrum. These pulses were attenuated in energy to 660 μJ and focused with a silver mirror with a radius of curvature (ROC) of -2000 mm into the first cell filled with Argon at an absolute pressure of 900 mbar. The output of the first filamentation stage exhibits a broadened spectrum, with its center of gravity shifted toward shorter wavelengths due to an ionization-induced blue-shift. Careful measurements yield an energy of 340 μJ in the central core, selected by an iris of 4 mm diameter placed at 140 cm from the focus position, which corresponds to an energy throughput of 51% after the first filamentation stage. The emerging pulses were measured with SPIDER after collimation and recompression with chirped mirrors [see Fig. 1(b)]. The measurement yields a 9.9-fs pulse corresponding to a compression factor of 3 when compared to the input pulse. The same process is repeated by refocusing these pulses with another silver mirror (ROC = -2000 mm) into the second gas cell filled with Argon at a pressure of 820 mbar. An iris in between the two stages is used to optimize the filament compression in the second cell. The spatial selection performed after the first cell does not correspond to the best one for the production of 10 fs pulses but corresponds to the best condition in the second cell to obtain the sub-5fs pulse. Under these conditions, a filament was formed in the second cell and spectral broadening of more than an octave was observed as previously reported in [10]. The full spectrum measured directly after the filamentation cell supports a sub-2-fs pulse. With subsequent chirped mirror compression and spatial selection of the beam core, we obtained in this experiment pulses as short as 4.9 fs with an energy of 70 μJ. This energy is lower in this experiment compared to our previous results because of the use of several dispersion-compensating elements without anti-reflection coating. The energy throughput is not limited by the filamentation process itself and can be improved to reach hundreds of μJ. Besides, the pulse duration is still limited by the bandwidth and the residual dispersion modulations of the chirped mirrors but it could also be improved by using specially designed chirped mirrors. Figure 1(c) shows the pulse measurement at different steps on the filamentation compression line.

#80983 - $15.00 USD Received 13 Mar 2007; revised 9 Apr 2007; accepted 10 Apr 2007; published 18 Apr 2007

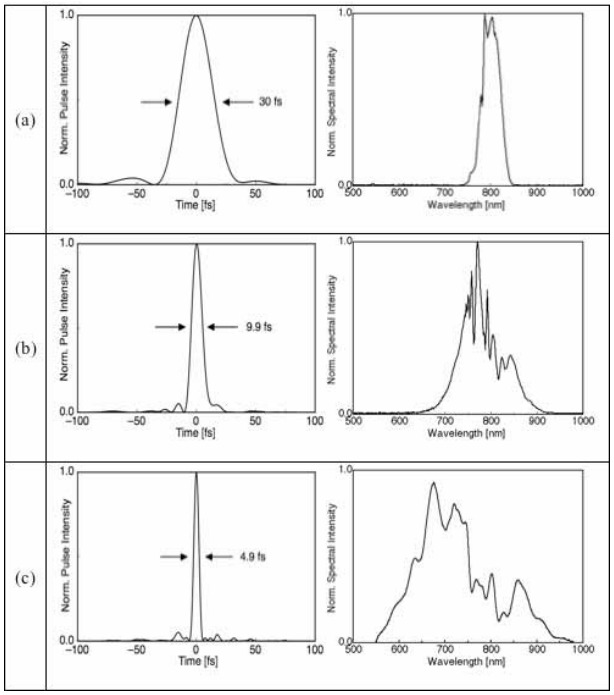

Fig. 1. Pulse shapes and associated spectra of (a) the input pulse (30 fs); (b) after the first filament cell (9.9 fs), and (c) after the second filament cell (4.9 fs).

A more detailed spatio-temporal characterization of the filament was performed by transversely scanning a 1-mm aperture in 100-μm steps through the 4 mm diameter output beam. The selected output beam is sent to the SPIDER in order to measure the transmitted temporal profile. Figure 2 shows the evolution of the temporal profile as a function of the transverse iris position in the output beam. A single 4.9-fs pulse can be measured only by selecting the center part of the beam. The temporal structure appearing on either sides of this short pulse remains below 10% of the peak intensity. Towards the outer parts of the beam, the temporal profile changes until a double pulse is formed. It is clear that without any spatial selection of the short pulse component, throughput is maximized at the expense of pulse contrast. Depending on the requirements for a particular application, one has to trade-off pulse duration versus contrast and energy throughput.

The pulses, both from the amplifier as well as those produced in the first and second filamentation stage, were used for HHG to investigate their usefulness for high-field physics experiments. The pulses were sent into a vacuum chamber where a synchronized 1-kHz pulsed jet was used for HHG in Argon. The beam was focused slightly in front of the jet to predominantly select the short quantum path [23, 24] and to observe a harmonic spectral broadening resulting only from the driving pulses. Figure 3 shows harmonic spectra corresponding to harmonics 15 to 29, measured for different pulse durations. The harmonic signal is plotted as a function of photon energy. As expected, significant broadening of the harmonic spectra is observed when using shorter pulses. Meanwhile a frequency shift occurs, which is attributed to the blue-shift of the driving pulse during filamentation. This blue-shift corresponding to 5 nm and 40 nm respectively after the first and the second filamentation stages, is converted linearly to the high order harmonic according to $\Delta E_q = q \times \frac{\Delta\lambda_0}{\lambda_0} \times \hbar\omega_0$,

#80983 - $15.00 USD Received 13 Mar 2007; revised 9 Apr 2007; accepted 10 Apr 2007; published 18 Apr 2007

where q is the harmonic order, ΔE_q is the harmonic blue-shift in eV, $\hbar\omega_0$ is the fundamental photon energy (at 795 nm $\hbar\omega_0 \approx 1.55eV$), λ_0 and $\Delta\lambda_0$ are the fundamental wavelength and blue-shift. For instance, the harmonic 21 shift changes from 0.21 eV (for the pulse obtained after the first filament stage) to 1.81 eV (for the pulse obtained after the second filament stage). More interestingly, the harmonics start to slightly overlap when generated with the sub-5-fs pulse, indicating that the presumable attosecond pulse train is composed of only a few attosecond pulses. Stabilizing the carrier-envelope offset phase [5,10,12] of such short pulses and performing a spectral selection of the harmonics generated could lead to the production of single attosecond pulses [3,7].

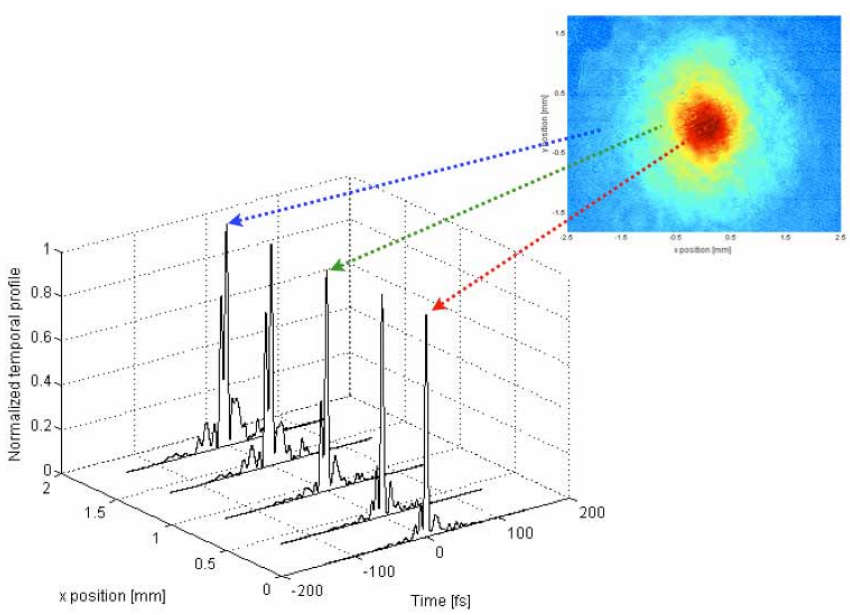

Fig. 2. Spatial dependence of the temporal profile measured at the output of the two-stage filamentation system. When the central part of the filament beam is selected, the profile corresponds to a single 4.9-fs pulse (at x=0 mm transverse position). Towards the outer part of the beam (x>0 mm transverse position), the energy is distributed on satellites structures leading to a double-pulse structure in the temporal profile.

#80983 - $15.00 USD Received 13 Mar 2007; revised 9 Apr 2007; accepted 10 Apr 2007; published 18 Apr 2007

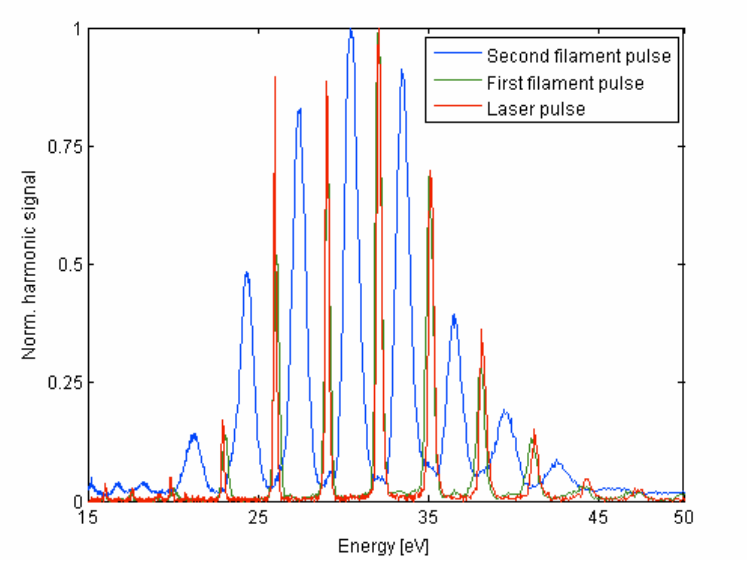

Fig. 3. Normalized harmonic signal versus photon energy for different driving pulse durations. The red line refers to the 30-fs pulse, the green line to the 10-fs pulse after the first filamentation stage, and the blue line to the sub-5-fs pulse obtained from the complete filamentation system.

To explain the experimental results, a theoretical investigation in space and time on pulse propagation through filamentation has been performed. We investigated the compression process on- and off-axis at the output of the filamentation stage to understand the spatial dependence of the temporal profile that leads to the double pulse structure.

3. Numerical simulation

The numerical code used for the simulation of filamentation was described in [11] and relies on the physical model developed for the propagation of an intense pulse in ionizing transparent media [25]. It solves the propagation equation for the envelope $E(r, t, z)$ of the laser pulse along the z-axis, coupled to the evolution equation for the plasma density $\rho(r, t, z)$, which read:

$$U\frac{\partial \varepsilon}{\partial z} = \frac{i}{2k_0}[\Delta_\perp + D]\varepsilon + N(\varepsilon) \tag{1}$$

$$\frac{\partial \rho}{\partial t} = \sigma_K |\varepsilon|^{2K}(\rho_{at} - \rho) + \frac{\sigma}{U_i}\rho|\varepsilon|^2 \tag{2}$$

Here $k_0 = k(\omega_0)$ denotes the wavenumber corresponding to the central frequency ω_0 and $k(\omega) = n(\omega)\,\omega/c$ where $n(\omega)$ is the refractive index of Argon. These equations are expressed in the reference frame moving with the pulse and thus, t denotes the retarded time $\tau - z/v_g$ and $v_g \equiv \partial\omega/\partial k|_{\omega_0}$ the group velocity.

On the right hand side of Eq. (1), the first term represents the beam diffraction, the second term D accounts for all dispersive terms and the third term accounts for various nonlinear effects. The operator $U \equiv 1 + (i/k_0 v_g)\partial/\partial t$ accounts for space-time focusing. D is defined from its Fourier transform in the frequency domain $\hat{D}(\omega) \equiv k^2(\omega) - k_0^2\hat{U}^2$, where $\hat{U} \equiv 1 + (\omega - \omega_0)/k_0 v_g$. Standard dispersive terms can be made apparent by a small $\omega - \omega_0$

#80983 - $15.00 USD Received 13 Mar 2007; revised 9 Apr 2007; accepted 10 Apr 2007; published 18 Apr 2007

expansion of $\hat{D}(\omega)/2k_0$; $k_0^{"}(\omega-\omega_0)^2/2+k_0^{'''}(\omega-\omega_0)^3/6+...$, where $k_0^{"}\equiv\partial^2 k/\partial\omega^2\big|_{\omega_0}$ and $k_0^{'''}\equiv\partial^3 k/\partial\omega^3\big|_{\omega_0}$ are the second and third order dispersive coefficients.

The incoming pulse is assumed to be Gaussian in time and space and its envelope is described by:

$$\varepsilon(r,t,z=0)=\varepsilon_0\exp\left(-\frac{r^2}{w_0^2}-\frac{t^2}{t_p^2}-i\frac{k_0 r^2}{2f}\right) \tag{3}$$

where w_0 is the beam waist, t_p is the pulse duration and f the effective focal length of the system.

The input intensity is computed from the input power $\varepsilon_0^2=2P_{in}/\pi w_0^2$ and the input power P_{in} is computed from the pulse energy $P_{in}=E_{in}/t_p\sqrt{\pi/2}$.

The last term in Eq. (1) represents nonlinear effects and it reads as:

$$N(\varepsilon)=i\frac{\omega_0}{c}n_2T^2|\varepsilon|^2\varepsilon-\frac{\sigma}{2}(1+i\omega_0\tau_c)\rho-T\frac{\beta_K}{2}(1-\frac{\rho}{\rho_{at}})|\varepsilon|^{2K-2}\varepsilon \tag{4}$$

The first term in Eq. (4) represents the optical Kerr effect where n_2 denotes the nonlinear refraction coefficient. Self-steepening is accounted through the operator $T\equiv 1+(i/\omega_0)\partial/\partial t$ in front of the Kerr term [26, 27]. The second term models absorption and defocusing due to the plasma generated in case the power P_{in} exceeds the critical threshold for self-focusing $P_{cr}=\lambda_0^2/(2\pi n_0 n_2)$. The last term describes nonlinear energy losses corresponding to the energy necessary for ionization. For short pulses of a few tenths of fs, optical field ionization is the dominating process for plasma generation in the filament. The results presented below do not critically depend on the choice of the ionization rate that has been retrieved by using the Keldysh formulation (see Ref. [25] for a presentation of the model in this case) or simply multiphoton ionization rates for Argon atoms with neutral density ρ_{at}, potential U_i and values given below.

The rate $W_K=\sigma_K I^K$ increases rapidly with intensity and the power $K=\mathrm{mod}(U_i/\hbar\omega_0+1)$ denotes the number of photons involved in the process (U_i = 15.76 eV and K = 11 at 800 nm). We also considered the inverse Bremsstrahlung process with a cross section of $\sigma=(e^2/n_0\varepsilon_0 m_e c)\times\tau_c/(1+\omega_0^2\tau_c^2)$ according to the Drude model, where τ_c denotes the collision time.

The parameters used in our simulations for Argon are the following at atmospheric pressure: (i) the frequency dependent refractive index is obtained by the Sellmeier-like dispersion relation [28]; (ii) the nonlinear refraction index n_2 = 3×10^{-19} cm^2/W was chosen so as to mimic the experimental observation of nonlinear focus and filamentation length. This value lies between those calculated from data in Ref. [29] and in Ref. [30]. At 795nm, this corresponds to P_{cr} = 3.4 GW. (iii) The multiphoton ionization coefficient is σ_K = 5×10^{-140} s^{-1}cm^{22}W^{-11}, which yields the multiphoton absorption coefficient $\beta_K=K\hbar\omega_0\rho_{at}\sigma_K$ = 3.4×10^{-138} cm^{19} W^{-10} for ρ_{at} = 2.5×10^{19} cm^{-3}. (iv) The collision time and the cross section for inverse Bremsstrahlung are τ_c = 190 fs and σ = 7.8×10^{-24} m^2, respectively. Finally, all coefficients are pressure dependent. All coefficients are roughly proportional to the pressure except for P_{cr} and τ_c which vary as p^{-1} [31].

The pulse parameters at the entrance window of the first gas cell are: w_0 = 2.7 mm, f=56cm, t_p = 25 fs (FWHM 30 fs). The parameter f correspond to the beam curvature at the entrance of the gas cell calculated from the experimental setup characteristics which induce a beam size

#80983 - $15.00 USD Received 13 Mar 2007; revised 9 Apr 2007; accepted 10 Apr 2007; published 18 Apr 2007

at the entrace given by w_0. We also performed simulations from the entrance of the second gas cell with t_p = 8.5 fs (FWHM 10 fs).

4. Numerical results

The panel in Fig. 4 shows the evolution of the spatio-temporal intensity distribution along the propagation distance in the first gas cell. Similar results are obtained for the second gas cell. The four selected figures highlight the pulse transformation from a typical V-shape at the beginning of the filamentation stage to the nearly single cycle central structure surrounded by extended conical feet beyond the filament. The pulse generates a plasma channel for distances 40 cm < z < 80 cm behind the entrance window of the cell. Figure 4(a) exhibits typical features reflecting the nonlinear dynamics at the beginning of the filamentation stage: the V-shaped most intense part results from the interplay between the strong transverse compression of the central time slices due to the Kerr effect and the plasma defocusing of the trailing time slices. In the second gas cell, we obtained additional ring structures for the central time slices around t = 0. They result from the modulational instability of the beam with power above P_{cr}, which tend to break-up the beam into beamlets, each carrying about one P_{cr}.

The effect of plasma defocusing on these rings is at the origin of the multiple cone formation for beams with peak power well above P_{cr} [32]. Figures 4(b) and 4(c) show that the conical components of the wavepacket further evolved into an intense central peak with duration of about 10 fs for the first gas cell (4 fs in the second gas cell) surrounded by weaker more or less conical feet. After the end of the filament, the wavepacket evolves nearly linearly under the effects of diffraction and dispersion. Figures 4(c)-4(d) show that the overall conical structure of the wavepacket is preserved. The wavepacket undergoes a spreading in space and to a smaller extent, in time. A possible explanation for the conservation of this pulse shape was given by the interpretation of filamentation in condensed media [33–36]: The pulse tends to reach stationarity and thus spontaneously reshapes into a conical wavepacket finally relaxing toward a linear-X mode, i.e. a non-diffractive and non-dispersive eigenmode of the medium which can be viewed as the spatiotemporal extension of a Bessel beam. Due to the finite energy content of the wavepacket, a true linear X-mode (which possesses an infinite energy as for the Bessel beam if it is not apodized), and thus stationarity is reached only partially.

#80983 - $15.00 USD Received 13 Mar 2007; revised 9 Apr 2007; accepted 10 Apr 2007; published 18 Apr 2007

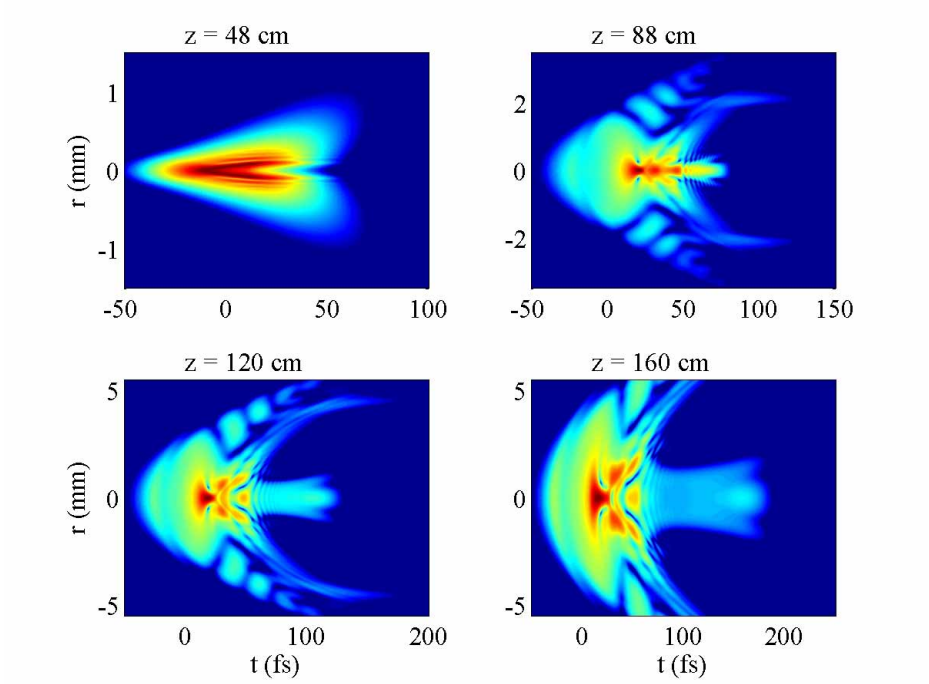

Fig. 4. Numerically computed spatiotemporal intensity distribution in the first gas cell. Log scale was used for all figures and the dynamic range of the colormap spans 4 decades. The distances are measured from the entrance window of the cell.

A natural interpretation of the double pulse structure observed in the spatially resolved pulse shape measurement follows directly from the simulations of this transformation into a conical wavepacket during filamentation. Figure 5 illustrates this interpretation with radially averaged temporal profiles of the wavepacket obtained in the second gas cell from numerical simulations, at a distance of 68 cm behind the entrance window. The plasma channel in the second gas cell is generated for 40 cm < z < 75 cm. In order to mimic the spatially resolved measurement of the pulse temporal structure, a 200-μm wide part of the intensity distribution is selected within the filament by means of a 'numerical slit' located at different radial distances from the propagation axis. A radial integration is then performed, thus resulting in averaged temporal profiles, which represent the power content of the beam at a given distance. Figure 5(a) shows the on-axis temporal profile of the pulse characterized by a 4-fs intense peak and a moderately intense pedestal. The presence of ripples in the trail of the pulse features an optical shock as also shown by the steep trailing front and indicates that this pulse is close to the shortest structure just formed by the filament. Figures 5(b)–5(d) show the averaged temporal profile obtained by moving the 'numerical slit' along the transverse axis. The averaged trailing pulse becomes longer and sub-pulses appear in the leading part. A double pulse structure is clearly visible farther from axis (450-650 μm). The comparison of this double pulse with the on-axis pulse supports the interpretation of each sub-pulse as a part of a biconical wavepacket in space and time.

#80983 - $15.00 USD Received 13 Mar 2007; revised 9 Apr 2007; accepted 10 Apr 2007; published 18 Apr 2007

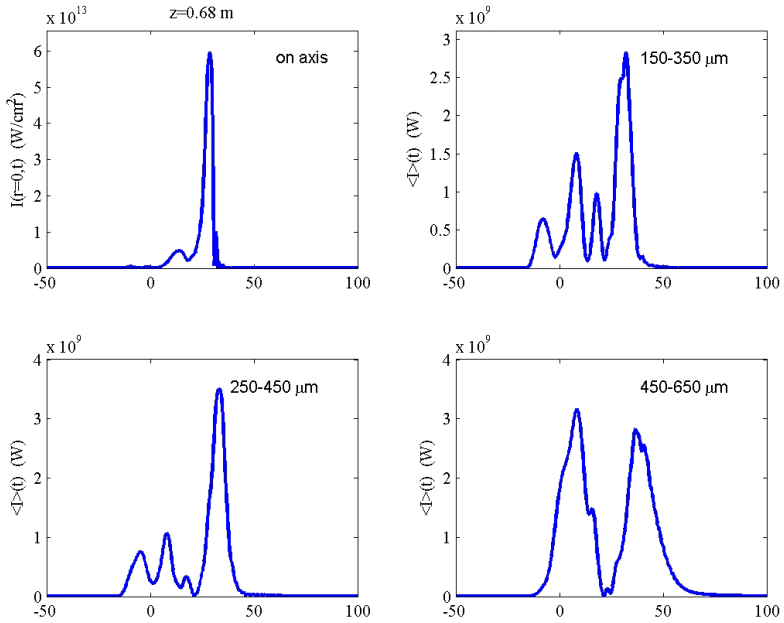

Fig, 5. (a). On axis and (b–d) radially averaged temporal profiles (time scale in fs) of the pulse apertured by a 'numerical slit' with boundaries indicated on each graph.

5. Conclusion

Sub-5-fs pulses were generated using filamentation in a noble gas atmosphere and subsequent compression with chirped mirrors. We have investigated experimentally and theoretically the spatial dependence of the filamentation output temporal profile. In particular we show that a selection of the output beam core part is a necessary condition to generate the shortest pulses. It is clear that depending on the applications requirement, a trade-off has to be made between the duration of the pulse and the energy available at the output of the filamentation stage. However, by selecting the inner part of the beam, pulses as short as 4.9 fs have been generated, with an optimized contrast, that contain sufficient energy to successfully produce high-order harmonics in Argon. Further significant improvements of the filamentation technique are expected from self-compression during propagation in a cell with a pressure gradient profile. A significant advantage of such a technique would be pulse compression into the single-cycle regime as it has been theoretically predicted in Ref. [16]. Propagation to a high harmonic chamber would then proceed in vacuum, hence preventing further dispersive broadening and rendering additional dispersion compensation unnecessary.

Acknowledgments

We acknowledge the financial support from the European Union FP6 program "Structuring the European Research Area" and the Marie Curie Research Training Network XTRA (contract FP6-505138) as well as from the Swiss National Science Foundation under their QP-NCCR initiative.
We acknowledge Dr. Philip Schlup from Colorado State University for providing the SPIDER software support.

[i] Curently at ICREA and ICFO - The Institute of Photonic Sciences, 08860 Castelldefels (Barcelona), Spain

#80983 - $15.00 USD Received 13 Mar 2007; revised 9 Apr 2007; accepted 10 Apr 2007; published 18 Apr 2007